Journal of Alloys and Compounds 511 (2012) 209–214

Contents lists available at SciVerse ScienceDirect

Journal of Alloys and Compounds

journal homepage: www.elsevier.com/locate/jallcom

Study of glass formation in the Sb_2O_3–PbO–MnO ternary system

M. Nouadji [a], A. Attaf [a], R. El Abdi [b,*], M. Poulain [c]

[a] Département de Physique, Université de Biskra, Biskra 07000, Algeria
[b] Larmaur, Université de Rennes1, CS 74205, 35042 Rennes Cedex, France
[c] Laboratoire Verres et Céramiques, Université de Rennes1, 35042 Rennes Cedex, France

ARTICLE INFO

Article history:
Received 5 July 2011
Received in revised form
13 September 2011
Accepted 14 September 2011
Available online 19 September 2011

Keywords:
Antimony oxide
Mechanical properties
Optical properties
Crack analysis

ABSTRACT

Vitreous systems based on antimony oxide Sb_2O_3 have been investigated. The influence of MnO substitution on the mechanical and physical properties in the $(80-x)Sb_2O_3$–20PbO–xMnO and $(70-x)Sb_2O_3$–$(30-x)$PbO–2xMnO systems has been studied. Vickers hardness, density, molar volume, Young modulus, glass temperature transition, infrared and UV transmission spectra depend on the MnO concentration. Crack analysis of the glass surface under indentor deformation shows the tenacity changes according to concentration of the MnO.

© 2011 Elsevier B.V. All rights reserved.

1. Introduction

Heavy metal oxide glasses (HMOG) make up an important group of special glasses that specifically are free of classic vitrifiers such as oxides of boron, silicon and phosphorus [1]. While this definition leads to a large variety of HMOG families based on V_2O_5 [2–5], Ga_2O_3 [1], MoO_3 [2,4], WO_3 [3], Bi_2O_3 [6], TeO_2 [7–9] and Sb_2O_3 [10–15] as main glass formers, generic research focuses rather on tellurites and antimonites. Germanate glasses – especially lead germanates – were developed a long time ago and are on the border line between silicates and HMOG [16]. By comparison to current oxide glasses, the general features of HMOG encompass low melting temperature, low phonon energy, extended IR transmission, high refractive index and large optical non linearity [8,11,17].

Antimonite glasses based on Sb_2O_3 have been the subject of various studies, mainly on alkali antimonites [10,18]. More numerous reports concern antimony oxyhalide glasses. They exhibit close similarities to tellurite glasses that have been more extensively studied. Metallic halide chloride can be incorporated in HMOG to obtain a very large subfamily [19].

Unfortunately, halide glasses usually exhibit a low level of mechanical properties and low thermal stability. Oxide glasses might be better because of their higher stability and mechanical properties. But for conventional oxide glasses up-conversion emissions are usually weak [20] and the development of rare earth doped low phonon oxide glasses like antimonite glasses has increased recently [21–24].

On the other hand, the study of oxychloride glasses in the Sb_2O_3–$SrCl_2$–$CdCl_2$ and Sb_2O_3–$SrCl_2$–$CdCl_2$ + 0.5$ZnCl_2$ ternary systems has been undertaken by Lezid and co-workers [25]. It has been shown that cadium has some glass forming ability and the $ZnCl_2$ enlarges the vitreous domain. The influence of tungsten ions on the physical properties of glass has been studied by Krishna and Rao [26]. The addition of tungsten ions on the ZnO–Sb_2O_3–As_2O_3 system undertaken [26] and leads to a strong degree of deformation in the glass network.

Binary glasses Sb_2O_3–$PbCl_2$ exhibit a good resistance to devitrification [11], but little information appears to be available about the Sb_2O_3–PbO association. Lead oxide is known to enhance vitrification and is assumed to act as a network modifier, although it may also enter the vitreous network [27]. This paper is centred on ternary glasses in the Sb_2O_3–PbO–MnO ternary system, with a special emphasis on mechanical properties. Manganese oxide has been chosen as the third component for future magnetic and spectroscopic measurements.

2. Experimental

Glass samples for this study were prepared from commercial starting materials: Sb_2O_3 ≥99% (Acros), PbO ≈99+% (Alfa Aesar) and MnO ≈99+% (Acros). Synthesis was carried out in several steps: the mixture of the calculated amount of powders was introduced into a silica or soda-lime glass tube of about 10 mm in diameter. Mean batch weight was around 5 g. Rapid melting was achieved by flame heating until a clear liquid was obtained. Following this, melt was cast onto a brass plate or squeezed between two metal plates. This plate was preheated to around 200 °C to

* Corresponding author. Tel.: +33 2 23 23 41 12; fax: +33 2 23 23 41 12.
E-mail address: relabdi@univ-rennes1.fr (R. El Abdi).

0925-8388/$ – see front matter © 2011 Elsevier B.V. All rights reserved.
doi:10.1016/j.jallcom.2011.09.037

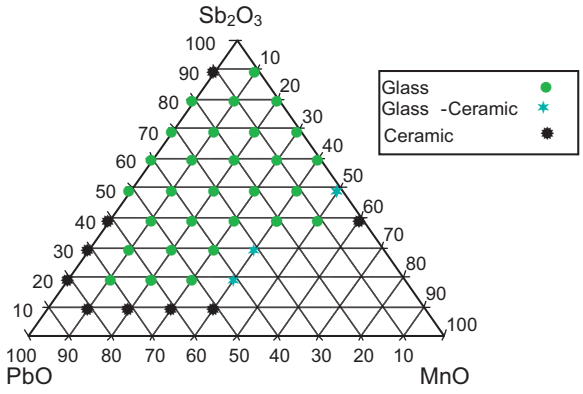

Fig. 1. Compositional limits for glass formation in the Sb_2O_3–PbO–MnO system.

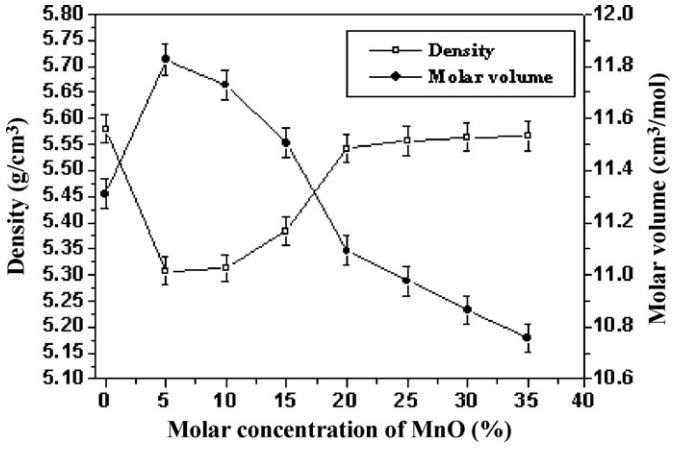

Fig. 2. Density and molar volume versus molar MnO concentration ($(80-x)Sb_2O_3$–20PbO–xMnO system).

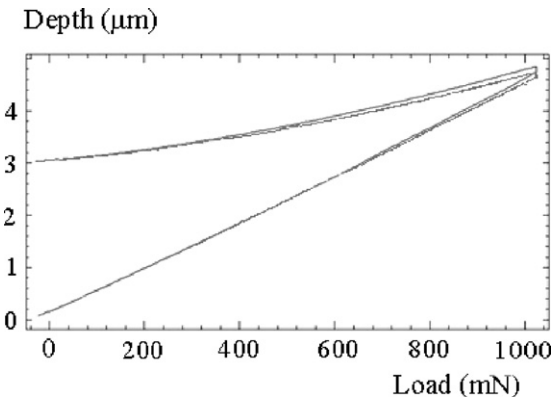

Fig. 4. Loading and unloading indentation curves for test reproducibility.

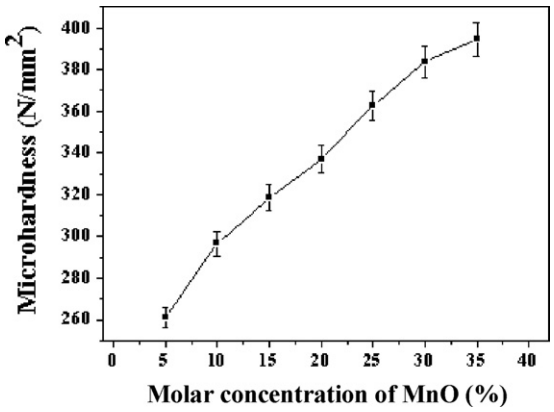

Fig. 5. Vickers hardness versus molar MnO concentration ($(80-x)Sb_2O_3$–20PbO–xMnO system).

obtain small discs that were polished for physical measurements. Estimated cooling rate ranges were from 10 to 100 K/s, resulting in samples a few mm in thickness.

Characteristic temperatures were measured by differential scanning calorimetry (DSC 2010 from TA Instruments) by heating at 20 K/min. Small bulk samples, 5–10 mg in weight, were set in aluminium sealed pans and positioned on the sample platform. The estimated temperature accuracy was ±2 K for the temperatures of glass transition T_g and the onset of crystallization T_x, and ±1 K for the temperature of the crystallization peak. The difference $T_x - T_g$ gives an estimate of stability against devitrification [28].

Optical transmission was recorded in the UV–visible spectrum and in the mid infrared, using a double beam spectrometer (Varian Cary 5) and a Bomem Michelson 100 IR spectrometer. The density was determined using a helium pycnometer (Micromeritics, AccuPyc 1330), with an accuracy of ±0.001 g/cm³. Ultrasonic measurements were performed by the pulse-echo method with a Panametrics model 5800 pulser/receiver with a quartz transducer. Both an X-cut transducer and a Y-cut transducer (with 10 MHz frequency) were employed for longitudinal modes and for shear modes. The pulse transient was measured with a Hewlett-Packard model 54502A oscilloscope. The uncertainty is estimated to be about ±1%.

The limits of the vitreous area of the Sb_2O_3–PbO–MnO system are shown in Fig. 1. These limits correspond to quenched glasses. Binary glasses are observed both with lead oxide and manganese oxide. Note that the lead concentration may be very high, close to 70 mol%. A large concentration of antimony oxide (>50 mol%) is required to obtain glass in the binary system Sb_2O_3–MnO.

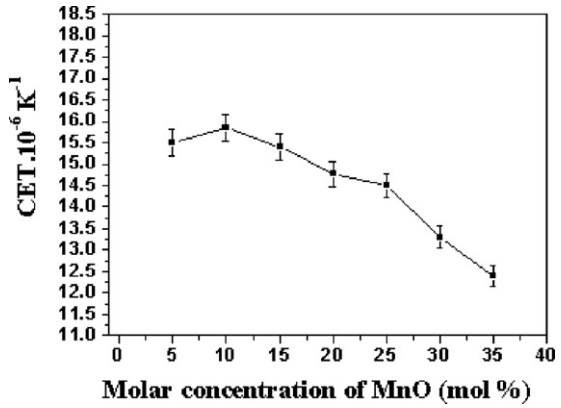

Fig. 3. Expansion coefficient for different MnO molar concentrations ($(80-x)Sb_2O_3$–20PbO–xMnO system).

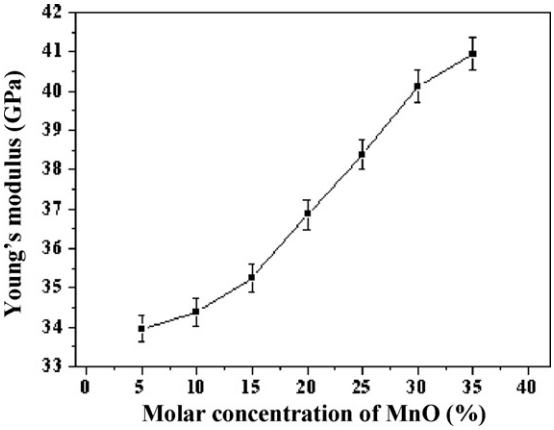

Fig. 6. Young modulus versus molar MnO concentration ($(80-x)Sb_2O_3$–20PbO–xMnO system).

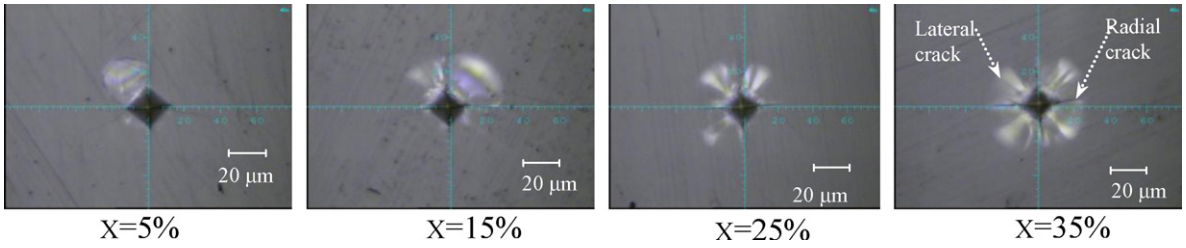

Fig. 7. Radial and lateral cracks for different MnO molar concentrations ($(80-x)Sb_2O_3$–20PbO–xMnO system).

3. Mechanical and optical testing results

While crystalline compounds have a well defined structure that does not change significantly when the component proportions vary in a limited way, vitreous systems are subject to structural modifications when the molar concentration changes.

Since the mechanical strength of a glass is determined by its surface characteristics, it is useful to ascertain the effect of the molar concentration of each vitreous system component on the mechanical behaviour with respect to changes in Young modulus, density, molar volume, hardness and material chipping. Table 1 gives the mechanical properties of each used component. Two vitreous systems have been studied:

- $(80-x)Sb_2O_3$–20PbO–xMnO (x = molar MnO concentration)
- $(70-x)Sb_2O_3$–$(30-x)$PbO–2xMnO

3.1. Study of $(80-x)Sb_2O_3$–20PbO–xMnO system

Fig. 2 gives the density and the molar volume versus the molar MnO concentration. Density analysis was obtained using a helium pycnometer. The molar PbO percentage is constant and equal to 20% for whatever the molar MnO concentration x was. When x increases from 0 to 5%, the system density decreases (Sb_2O_3 density is higher than that of MnO, Table 1). When the MnO concentration increases above 5% (5% < x < 40%), the density increases. This may be explained as an intercalation process of ionic species (Mn^{2+} and O^{2-}) between Sb_2O_3 layers. The electrostatic interaction between O^{2-} anions and Mn^{2+} cations increases the stability of the system.

Conversely, Fig. 2 gives an opposite change of the molar volume since volume and density vary in an opposite way:

$$\text{Molar volume} = \frac{\text{Molar mass}}{\text{Density}} \quad (1)$$

Another measurement of the thermal expansion coefficient helps to explain the molar volume behaviour according to the MnO concentration. Indeed, Fig. 3 shows that the expansion coefficient increases for low MnO concentrations, and then it decreases inducing a molar volume decrease for the studied system.

To characterize the hardness and the deformation mode of the glass surface, the indentation hardness technique was used. When a sharp indenter, such as the Vickers indenter, is loaded onto a material, a residual surface impression is observed after unloading, and the material hardness is generally estimated from the projected area of the impression. The deformation is dependent on the applied load, temperature and load time.

Table 1
Mechanical properties of used materials.

Components	Density (g/cm^3)	Molar weight (g/mol)	Vickers hardness (N/mm^2)	Molar volume (cm^3/mol)
PbO	9.64	223.2	60	23.15
MnO	5.37	70.94	530–820	13.21
Sb_2O_3	5.75	291.4	60–100	50.68

Indentation experiments were performed with a Vickers diamond indenter. Vickers diamond pyramid hardness was determined in practice by measuring the diagonal length of the indentation produced by the penetration of a square-based pyramid having an angle of 136° between opposite pyramid faces. The hardness number HV is given by the equation:

$$HV = \frac{0.1891F}{d^2} \quad (\text{in N/mm}^2) \quad (2)$$

F is the applied load, and d is the average length of the square diagonal which is left by the indenter.

Although the diagonal d, in Eq. (2) is obtained by measurement after the removal of the load, it is known that the change in the lengths of the diagonals upon unloading is very small [29] and almost insignificant when compared to the diagonal length itself.

The Vickers hardness was calculated for each sample using the average residual area of 9 indentations.

On the other hand, the indentation test is carried out twice in order to analyze the loading curve reproducibility (Fig. 4). One can note that the tangent to the unloading curve at the beginning of unloading gives the Young modulus value. Fig. 4 shows that the maximum applied load for all samples is about 1 N.

The manganese oxides have a rather high level of hardness (Vickers hardness between 530 and 820 MPa, Table 1) which corresponds to Mohs hardness between 5 and 6 (limited to 10 for diamond). The increase in MnO concentration leads to a microhardness increase and to a Young's modulus increase (Figs. 5 and 6).

Manganese oxide is the most important manganese compound and is a brittle metal element. When the MnO molar concentration increases, the hardness and the brittleness of the vitreous system increase leading to an increase in the number of lateral cracks (Fig. 7).

A radial crack appears at the edge of the indenter print and leads to a lateral crack at the square sides of the print. Fig. 7 shows that a MnO rate of 5% leads to a lateral crack on only one edge of the print and an MnO content of 35% gives lateral cracks on all the print edges.

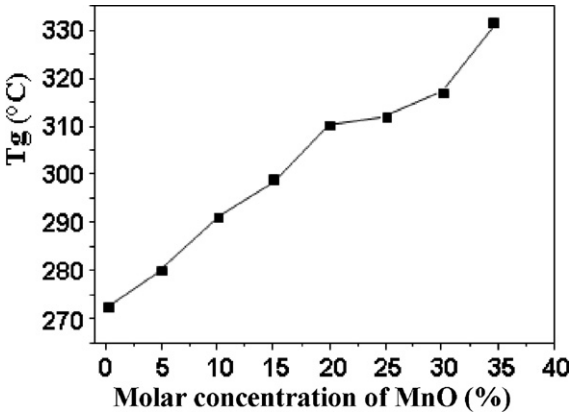

Fig. 8. Glass temperature transition T_g versus molar MnO concentration ($(80-x)Sb_2O_3$–20PbO–xMnO system).

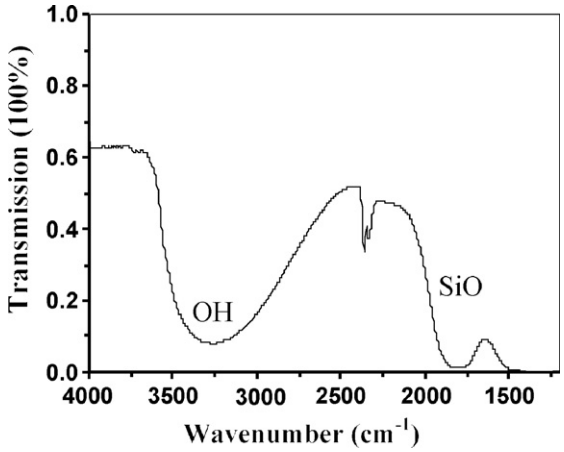

Fig. 9. Infrared transmission spectrum of $(80-x)Sb_2O_3$–20PbO–xMnO systems for different MnO molar concentrations (sample thickness: 2 mm).

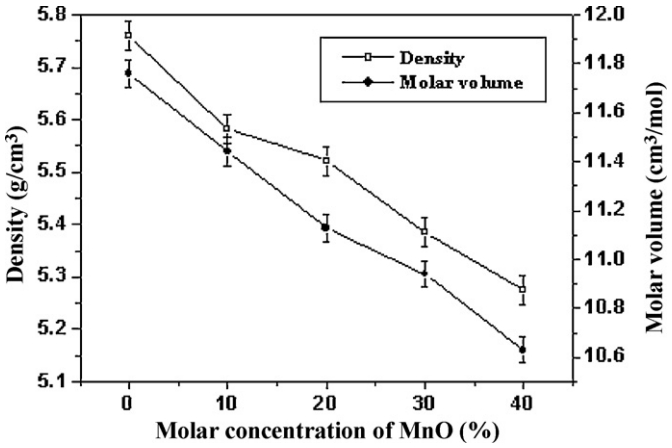

Fig. 12. Density and molar volume versus molar MnO concentration ($(70-x)Sb_2O_3$–$(30-x)$PbO–2xMnO system).

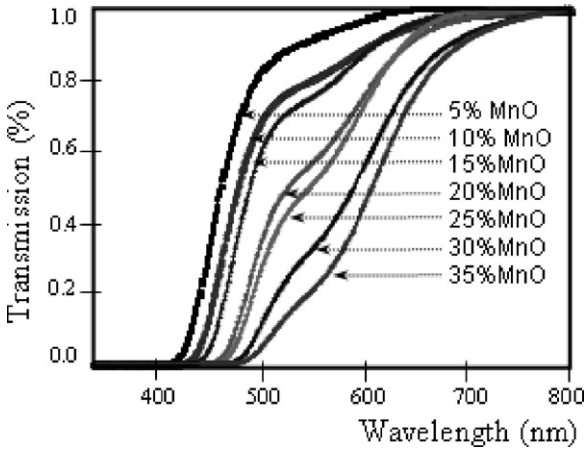

Fig. 10. UV transmission spectra of $(80-x)Sb_2O_3$–20PbO–xMnO systems for different MnO molar concentrations (sample thickness: 2 mm).

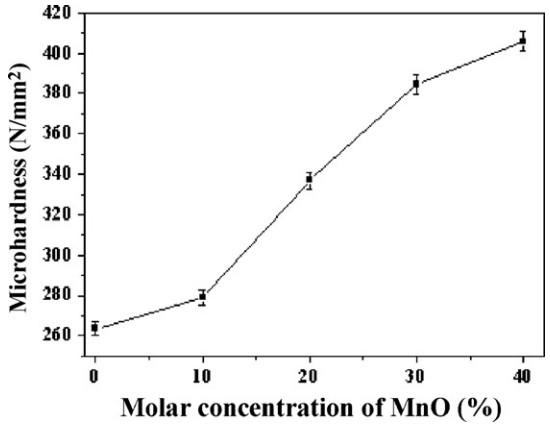

Fig. 13. Vickers hardness versus molar MnO concentration ($(70-x)Sb_2O_3$–$(30-x)$PbO–2xMnO system).

The MnO content increase does not lead to larger lateral cracks (all lateral cracks have a circular form with a radius of approximately 30 μm) but to a larger number of lateral cracks which surround the print. This can result in the fact that the greater the MnO content, the greater the decrease in the tenacity of the system leading to internal cracks, which may connect, and of producing other lateral cracks.

Thermal properties are measured by differential scanning calorimetry with heating at 20 K/min. The changes of glass temperature transition T_g manganese monoxide, according to chemical content, is shown in Fig. 8. The general trend is that T_g increases as manganese monoxide substitutes for antimony oxide.

Infrared and UV–visible transmission measurements were undertaken.

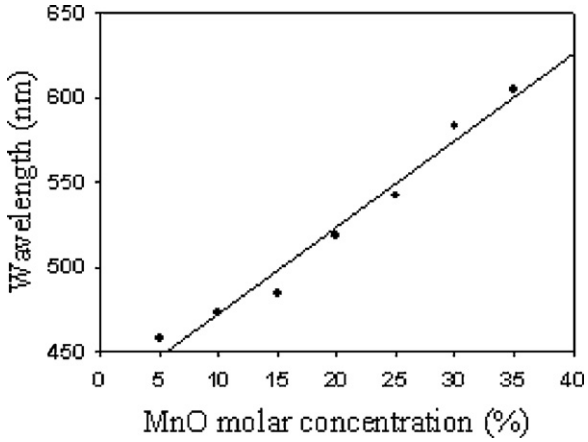

Fig. 11. Wavelength versus MnO molar concentration for UV–visible cut-off wavelength at 50% transmission.

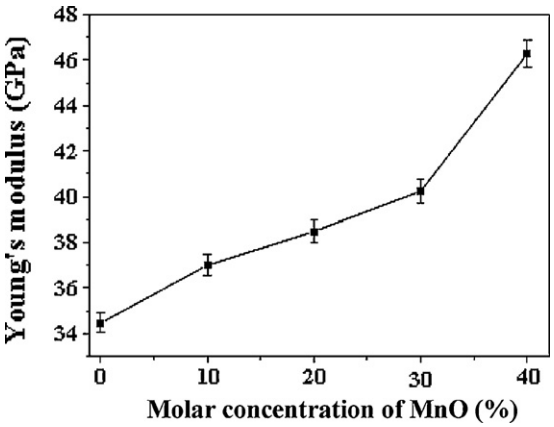

Fig. 14. Young modulus versus molar MnO concentration ($(70-x)Sb_2O_3$–$(30-x)$PbO–2xMnO system).

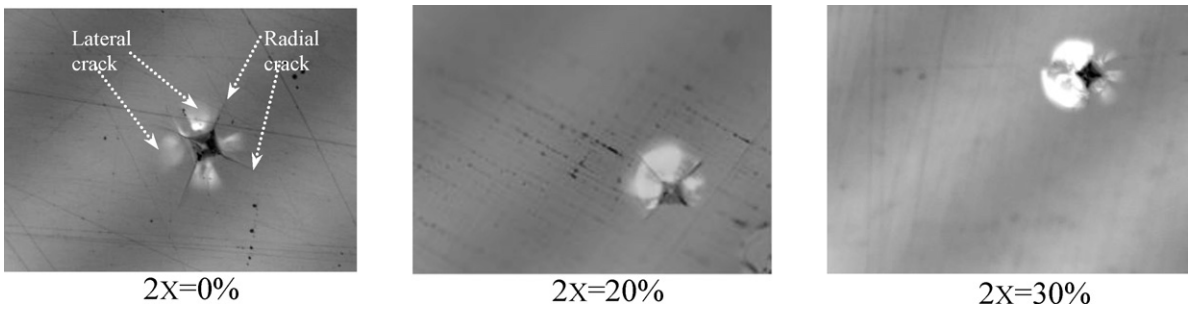

Fig. 15. Radial and lateral cracks for different MnO molar concentrations ($(70-x)Sb_2O_3$–$(30-x)$PbO–$2x$MnO system).

Figs. 9 and 10 give the infrared and UV transmission respectively. For a molar concentration of 5% MnO, in Fig. 9 one can observe the extrinsic absorption bands in the infrared spectrum: OH and SiO. The processing conditions i.e. room atmosphere and silica crucible, lead to obtaining these groups. One obtains the same behaviour when the molar concentration of MnO changes. Conversely, the UV spectrum (Fig. 10) shows the shift of the UV visible absorption edge with increasing manganese content. In oxides, Mn^{2+} ions are classically located in octahedral sites. The local field leads to various energy levels, which result in three main absorption bands between 300 nm and 600 nm.

Using the results from Fig. 10, when the transmission is equal to 50%, the wavelength presents a linear regression according to the molar concentration of MnO (Fig. 11).

3.2. Study of $(70-x)Sb_2O_3$–$(30-x)$PbO–$2x$MnO system

For the $(70-x)Sb_2O_3$–$(30-x)$PbO–$2x$MnO system, the PbO content varies with the MnO concentration.

The density of the system decreases due to the higher value of PbO density (Table 1) (when x increases, the PbO part decreases in the system $(70-x)Sb_2O_3$–$(30-x)$PbO–$2x$MnO) (Fig. 12).

In addition, Table 1 shows that Sb_2O_3 and PbO have a high molar weight (compared with that of MnO). Thus, when the MnO content x increases a severe reduction in the molar mass of the system is obtained. Since the density decreases as well as the molar mass of the system, a decrease in molar volume is observed (Fig. 12).

As for the case of $(80-x)Sb_2O_3$–20PbO–xMnO systems, the high MnO Vickers hardness values (Table 1) lead to an increase of microhardness as well as an increase in Young modulus versus the molar concentration MnO (Figs. 13 and 14).

The radial crack length decreases when the PbO molar concentration decreases, then the radial cracks disappear when the molar concentration of PbO is equal to or lower than 15% ($x = 15\%$) (Fig. 15).

Unlike the $(80-x)Sb_2O_3$–20PbO–xMnO systems for which the PbO content rate remained constant, for the $(70-x)Sb_2O_3$–$(30-x)$PbO–$2x$MnO systems, the molar concentration of PbO (and that of Sb_2O_3) decreases when the amount of x increases. However, these two components (Sb_2O_3 and PbO) have molar volumes which are higher than that of MnO (Table 1). When the concentration x increases, the obtained systems comprise an increasing number of moles with a smaller volume, which increase the material tenacity and reduce the defect sizes.

4. Conclusions

Vitreous systems based on antimony oxide Sb_2O_3 have been investigated. Binary glasses both with lead oxide and manganese oxide are obtained. The changes of mechanical and physical properties with respect to the composition have been studied in the series of $(80-x)Sb_2O_3$–20PbO–xMnO and $(70-x)Sb_2O_3$–$(30-x)$PbO–$2x$MnO systems. Young modulus as well as the hardness increases according to the concentration of MnO, since MnO hardness is high compared to that of both Sb_2O_3 and PbO.

For the $(80-x)Sb_2O_3$–20PbO–xMnO system, changes in density vary with the MnO concentration and an intercalation process of the ionic species (Mn^{2+} and O^{2-}) between Sb_2O_3 layers occurs. The T_g temperature is between 270 °C and 330 °C and has a practically linear behaviour. When the MnO concentration changes, a decrease in UV transmission is observed with an inflection of the curve towards lower wavelengths. The greater the increase in the concentration of MnO, the greater the number of lateral cracks around the indentor print with an increase in glass hardness. For the $(70-x)Sb_2O_3$–$(30-x)$PbO–$2x$Mno system, one obtains an increase of the number of lateral cracks with an increase in the MnO concentration and at the same time the radial microcrack lengths decrease and thus lead to an increase in glass tenacity.

Finally, this study showed the interest of MnO which can lead to optimized glasses for various applications.

References

[1] W.H. Dumbaugh, J.C. Lapp, J. Am. Ceram. Soc. 75 (1992) 2315–2326.
[2] R. Iordanova, V. Dimitrov, Y. Dimitriev, D. Klissurski, J. Non-Cryst. Solids 180 (1994) 58–65.
[3] B. Aitken, M. Djeneka, Tungstate, molybdate, vanadate base glass, US patent No. 6,376,399B (2002).
[4] Y. Taibi, M. Poulain, R. Lebullenger, L. Atoui, M. Legouera, J. Optoelectron. Adv. Mater. 11 (2009) 34–40.
[5] G.D. Khattak, N. Tabet, J. Electron. Spectr. Relat. Phenom. 136 (2004) 257–264.
[6] W.H. Dumbaugh, Phys. Chem. Glasses 19 (1978) 121–125.
[7] R. El Mallawany, Tellurite Glass Handbook, CRC Press, Boca Raton, USA, 2002.
[8] J.S. Wang, E.E. Vogel, E. Snitzer, Opt. Mater. 3 (1994) 187–203.
[9] C.J. Hill, A. Jha, J. Non-Cryst. Solids 353 (2007) 1372–1376.
[10] A. Winter, Verres Refract. 36 (1982) 353–356.
[11] B. Dubois, H. Aomi, J.J. Videau, J. Portier, P. Haggenmuller, Mater. Res. Bull. 19 (10) (1984) 1317–1323.
[12] M. Nalin, M.J. Poulain, M.A. Poulain, S.J.L. Ribeiro, Y. Messaddeq, J. Non-Cryst. Solids 284 (2001) 110–116.
[13] G. Poirier, M.A. Poulain, M.J. Poulain, J. Non-Cryst. Solids 284 (2001) 117–122.
[14] B.V. Raghavaiah, N. Veeraiah, J. Phys. Chem. Solids 65 (2004) 1153–1164.
[15] M.T. Soltani, T. Djouama, A. Boutarfaia, M. Poulain, J. Optoelectron. Adv. Mater. Symp. 1 (2009) 339–342.
[16] K. Nassau, D.L. Chadwick, J. Am. Ceram. Soc. 65 (1982) 486–491.
[17] R.E. de Araujo, C.B. de Araujo, G. Poirier, M. Poulain, Y. Messaddeq, Appl. Phys. Lett. 81 (2002) 4694–4696.
[18] M.T. Soltani, A. Boutarfaia, R. Makhloufi, M. Poulain, J. Phys. Chem. Solids 64 (2003) 2307–2312.
[19] M.A. Poulain, M. Matecki, J.L. Mouric, M.J. Poulain, Mater. Res. Bull. 18 (1983) 631–636.
[20] X. Pan, J. Yu, Y. Liu, S. Yoda, H. Yu, M. Zhang, F. Ai, F. Jin, W. Jin, J. Alloys Compd. 509 (2011) 7504–7507.

[21] J. Jakuti, L. Gomes, C.T. Amancio, L.R.P. Kassab, J.R. Martinelli, N.U. Wetter, Opt. Mater. 33 (2010) 107–111.
[22] K. Li, H. Fan, G. Zhang, G. Bai, S. Fan, J. Zhang, L. Hu, J. Alloys Compd. 509 (2011) 3070–3073.
[23] X.P. Jiang, Z.M. Yang, T. Liu, S.H. Xu, J. Appl. Phys. 105 (2009) 103–113.
[24] R. Xu, Y. Tian, M. Wang, L. Hu, J. Zhang, Opt. Mater. 33 (2011) 299–302.
[25] M. Lezid, M. Legouera, F. Goumeidane, M. Poulain, V. Nazabal, R. Lebullenger, J. Non-Cryst. Solids 357 (2011) 2984–2988.
[26] S.B.M. Krishna, D.K. Rao, J. Alloys Compd. 509 (2011) 7373–7380.
[27] A. Winter, J. Am. Ceram. Soc. 40 (1957) 54–58.
[28] A. Dietzel, Glasstech. Ber. 22 (1968) 41–50.
[29] M. Petzold, J. Landgraf, M. Füting, J.M. Olaf, Thin Solid Films 264 (1995) 153–158.